Title: Selective depolymerization of polyolefin plastics into olefin monomers on electrified tungsten filament

Authors: Shijie Yu[1], Haoyue Li[1], Sikai Wang[1], Ning Yan[1,2]*

Affiliations:

[1]Department of Chemical and Biomolecular Engineering, National University of Singapore, Singapore 117585, Singapore

[2]Centre for Hydrogen Innovations, National University of Singapore, Singapore 117585, Singapore

*Corresponding author. Email: ning.yan@nus.edu.sg

Abstract: Polyolefin plastics account for ~60% of global plastic waste, and thus depolymerizing large quantities of waste polyolefin plastics into olefin monomers is attractive for both recycling plastics in a circular economy and providing sustainable raw materials for the chemical industry. However, the selectivity of olefin monomers is limited even with catalysts. Here we report an electrified tungsten filament method for depolymerizing polyolefin plastics into olefin monomers with competitive selectivities. In this system, a high temperature zone exceeding 1000 °C enables plastic depolymerization within 1 s, while the flow field transfers the products to a zone near room temperature, preventing nonselective further conversion. For depolymerizing polyethylene to ethylene, this method achieves a selectivity of 48%, substantially improved compared with that of traditional methods, such as catalytic pyrolysis (typically <20%). Moreover, polyethylene and polypropylene of various molecular weights and their mixtures have been depolymerized with monomer selectivities of 45–58% without the formation of tars and chars. This strategy offers rich possibilities for advancing a circular economy based on waste plastics.

Introduction

Plastic products are ubiquitously used to bring great convenience to modern society, but they also pose non-negligible environmental and health problems (*1-3*). It is estimated that millions of tons of plastic waste enter the oceans every year, forming a massive plastic garbage belt that has a devastating impact on marine ecosystems (*4, 5*). In terrestrial ecosystems, plastic waste destroys soil structure, hinders plant growth, and affects the balance and stability of the entire ecosystem (*6*). Moreover, plastic pollution may pose a potential threat to human health, as humans ingest microplastics entering the ecosystem through food and water (*1, 7*). The most dominant disposal methods for plastics are still landfills and incineration, which either cause direct pollution or have a high carbon footprint (*8-11*). Recycling plastics through mechanical recovery avoids these problems, but the recycled plastics have compromised properties and are difficult to meet the demands of regular use (*12-14*). Chemical recycling of plastics, i.e., converting plastics into their monomers and then re-polymerizing the monomers, on the other hand, is an approach that offers reliable product properties (*12, 15-18*). Along this line, exciting advances have been reported, such as depolymerization of polyethylene terephthalate by enzymatic hydrolysis (*19-21*) or biomimetic binuclear catalysts (*22*) to obtain monomers.

However, in the case of waste polyolefin plastics, such as polyethylene (PE) and polypropylene (PP), the stable $C(sp^3)$–$C(sp^3)$ bonds and the lack of available selective breaking sites, along with the heat-absorbing nature of C–C bond cleavage, make the processes thermodynamically unfavorable at low temperatures (*23, 24*), and the selective regeneration of monomers difficult (*25-27*). Therefore, the conversion of polyolefins usually requires stringent reaction conditions, such as high temperature and/or long reaction time, which also exacerbate side reactions leading to low selectivity towards desired monomers (*28, 29*). Since the reaction network of the depolymerization process grows exponentially as the reaction proceeds, conventional thermocatalytic strategies to modulate the large number of reaction intermediates in the process are also challenging. Even with catalysts, the lack of selective breaking sites in the C–C bond structure and the complexity of reaction network lead to the selectivity being still limited (*17, 30, 31*). Essentially, the difficulty with low selectivity lies in the contradiction between the need for high temperatures to overcome the reaction energy barriers, and the fact that high temperatures simultaneously lead to the reconversion of the depolymerization products non-selectively.

Here, we report an electrified tungsten filament depolymerization strategy for selectively converting polyolefin plastics into monomers. Drawing inspirations from the thermal properties of light bulbs, we construct a tungsten filament reactor featuring ultra-fast heat transfer and multi-temperature zones, in which heat can excite and drive the flow field in both axial and radial directions, forming a reversed temperature and flow field. The polyolefin plastics, coated on the tungsten filaments and activated by joule heating, rapidly depolymerize upon contact with the filament's hot surface, and the decomposed products are immediately removed from the high-temperature zone, preventing secondary reactions and enhancing selectivity. Taking the depolymerization of PE as an example, our process achieves a monomer selectivity of about 48%, more than two times higher compared to conventional thermocatalytic processes. Moreover, by comparing the surface area normalized activity of the tungsten filament to that of conventional catalysts, our method realizes a C_2H_4 formation rate of up to 4×10^5 mmol m^{-2} h^{-1}, improving by more than two orders of magnitude.

Results

Design principle of the depolymerization strategy on electrified tungsten filament

Light bulb, which consists of structural units such as glass chamber, tungsten filament, and inert gas atmosphere, is a common household appliance used to produce light accompanied by heat (Fig. 1A). When the bulb is off, glass chamber, tungsten filament, and inert gas are all at room temperature. When a light bulb is turned on, the tungsten filament instantly (usually < 1 μs) generates a temperature of over 1000 °C, which is the origin of its luminosity. The lighting process of the tungsten filament is an ultra-fast heat transfer process, allowing for a significant heating rate of the tungsten filament (> 10^9 °C s^{-1}). Meanwhile, the glass chamber remains at near room temperature, while the intervening inert gas creates a temperature field with a sharp temperature gradient. Based on the different temperatures of the tungsten filament, glass chamber, and inert gas, a multi-temperature zone is spontaneously formed inside the light bulb at the instant the bulb is turned on.

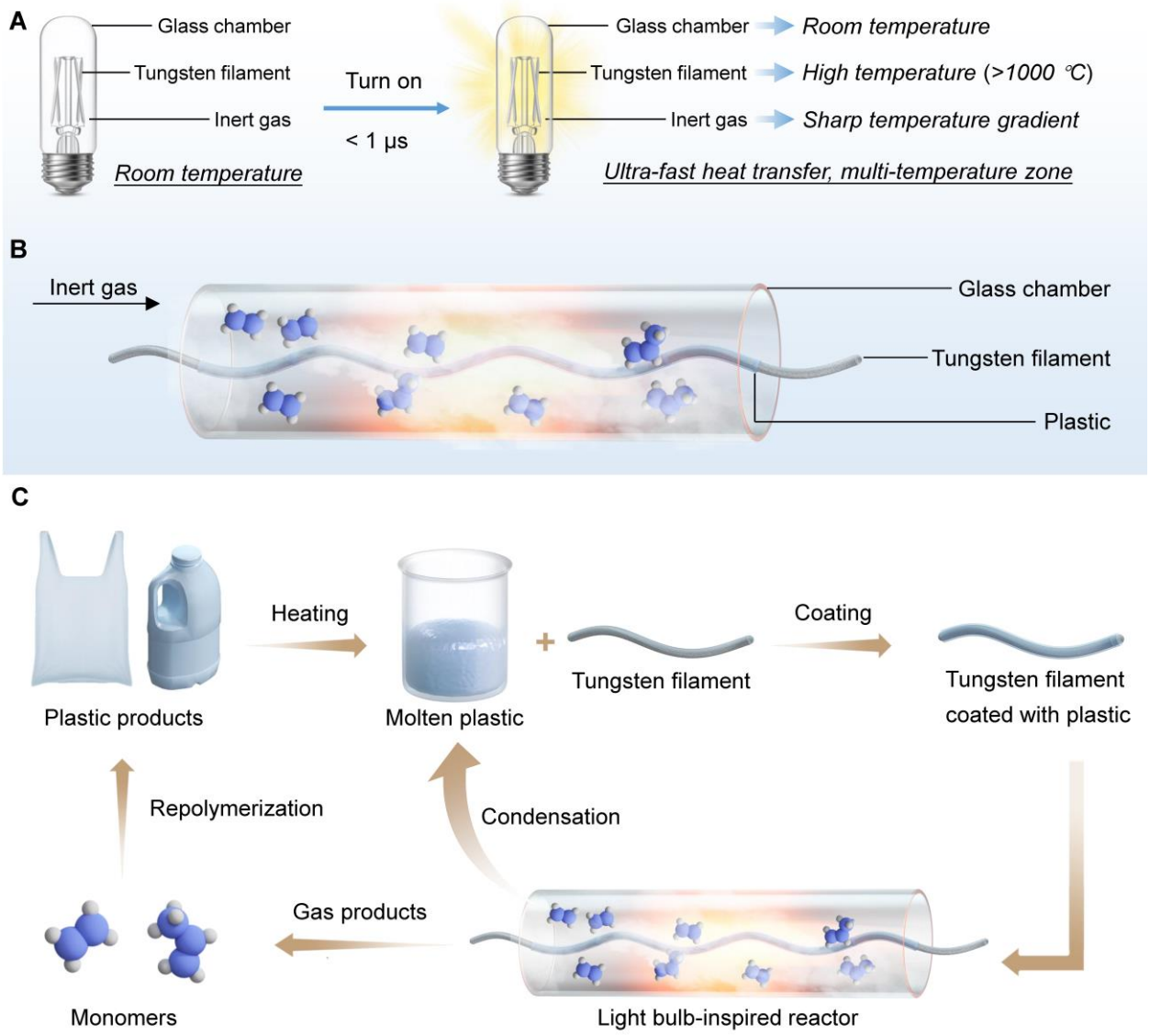

Fig. 1. Design framework of the depolymerization of polyolefin plastic by a light bulb-inspired reactor. (**A**) Schematic illustration of different constructions of a light bulb and principles of temperature variation when it is turned on. (**B**) Design and structure of a light bulb-inspired reactor. (**C**) Technological route of assembly and depolymerization of plastic in the light bulb-inspired reactor. The assembly process involves the heating and melting of the plastic, and

the coating of the molten plastic onto a tungsten filament. The depolymerization process consists of mounting the tungsten filament coated with plastic to the center of the light bulb-inspired reactor, flowing an inert gas through the reactor, and lighting the light bulb-inspired reactor. Plastic products, molten plastic, and plastic coating are labeled light blue for visual guidance and have no practical meaning.

Inspired by the dual properties of ultra-fast heat transfer and multi-temperature zone of the light bulb, we combined these potential advantages into a reactor for the depolymerization of polyolefin plastics (Fig. 1B). The unique property of ultra-fast heat transfer can serve as a reaction environment capable of avoiding the undesired side reactions triggered by the traditionally slow heating process of polyolefin plastics. Besides, the multi-temperature-zone environment created by the bulb potentially provides favorable conditions for controlling and stopping secondary reactions in the depolymerization of polyolefin plastics (see Fig. 3 for detailed discussion). Further, we introduce a flowing inert gas (e.g., argon) to create a characteristic flow field opposite to the temperature, which in turn enables the transport and control of plastics between different temperature zones. To enable a rapid heating rate, the polyolefin plastic needs to be deposited on the surface of the tungsten filament prior to depolymerization. Notably, polyolefin plastics are inherently thermoplastic, which means that they can be heated to a molten state (Fig. 1C), and then coated onto the tungsten filament. Using our light bulb-like reactor (fig. S1), the plastic-coated tungsten filament started to be lit up, and the plastic on the surface was molten, evaporated, and degraded instantly.

Depolymerization performance of polyethylene into ethylene

In a proof-of-concept experiment, a low-molecular-weight PE (~5 mg, $M_w = 5.2 \times 10^3$ g mol^{-1}, polydispersity $Đ = 4.1$) was coated on a tungsten filament (diameter $d = 0.1$ mm, length $l = \sim 160$ mm) and converted inside the light bulb-inspired reactor. After ~10 seconds with an operating temperature of ~1250 °C for tungsten filament (movie S1), the light bulb was turned off. The actual reaction time was within 1 second as recorded in the video, and the rest of the time was used to maintain the flow field for mass transport. During the operation period, the gas products were carried out of the reactor by an inert gas and collected. We used gas chromatography with flame ionization detection (GC-FID) to analyze the composition of gas products (Fig. 2A). After a typical reaction, we realized a high C_2H_4 selectivity of ~48%, accompanied by the production of other light hydrocarbons (e.g., CH_4, C_2H_6, C_3H_6, and C_3H_8). C_3H_6 was the second largest component of the gas products with a selectivity of about 14%, while the C_1–C_3 alkanes accounted for about 12%. The setting of the operating temperature is critical as it affects not only the physicochemical process of converting PE to C_2H_4, but also the secondary conversion of C_2H_4 (figs. S2 and S3). The operating temperature needs to be kept at a moderate level (1250 °C) because lower temperatures lead to slow reaction kinetics while higher temperatures promote the conversion of C_2H_4 to other hydrocarbons (e.g., cracking to CH_4 and dehydrogenation to C_2H_2), decreasing selectivity.

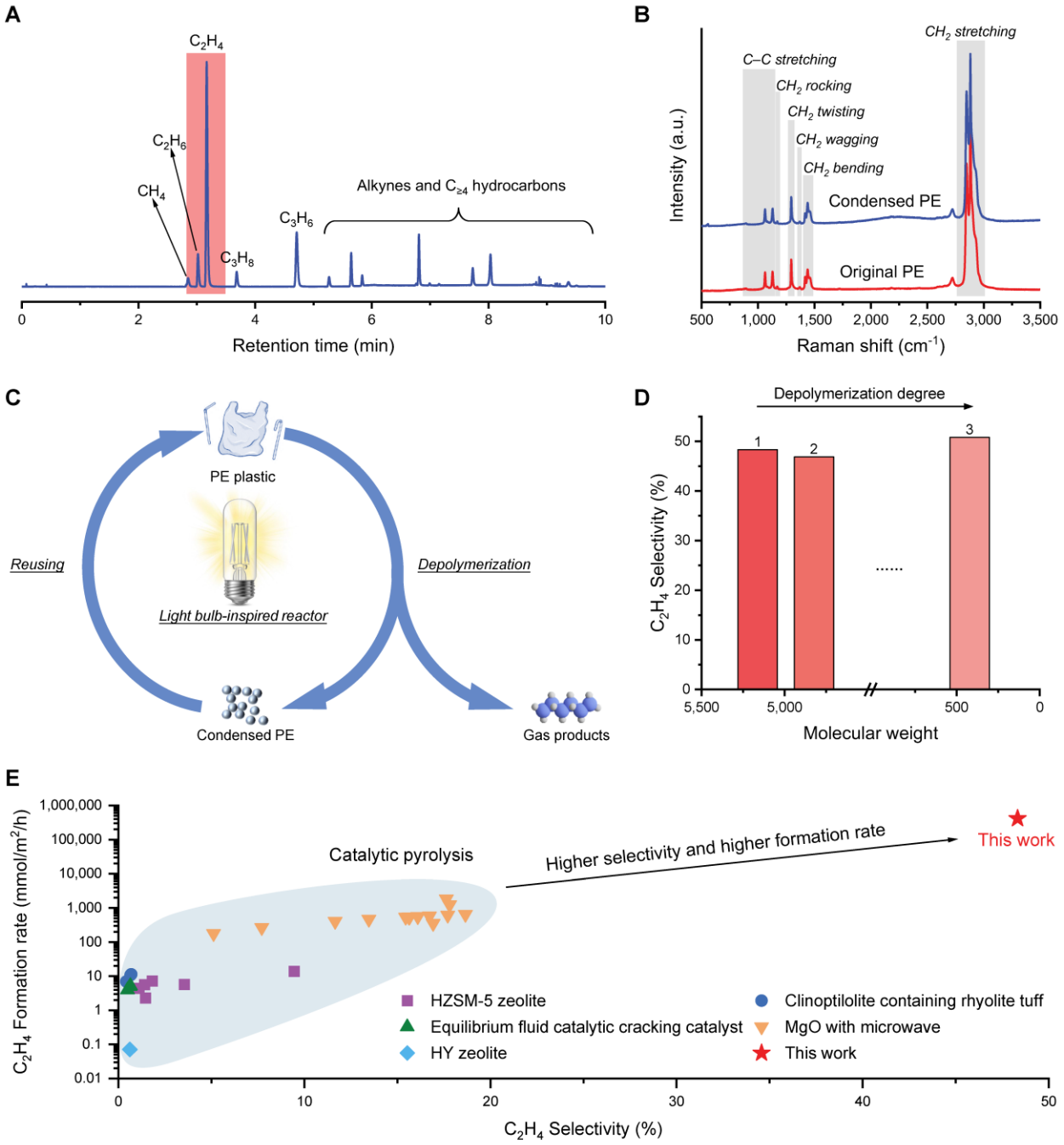

Fig. 2. Depolymerization of PE plastic via electrified tungsten filament approach. (**A**) Representative gas product distribution measured by gas chromatography with GC-FID. The pale red rectangle is present only to guide the eye. (**B**) Structural resolution of original PE and condensed PE by Raman spectroscopy (see table S2 for detailed band assignments). (**C**) Circular route map for the depolymerization of PE plastics by means of a light bulb-inspired reactor. During the depolymerization process, part of the PE plastic is converted to the target gas product, while part of the PE plastic is condensed down under control to achieve high selectivity in the depolymerization process. The condensed PE plastic can then be reconverted until all of it is fully valorized into highly selective gas products. (**D**) C_2H_4 monomer selectivity of PE or PE model compound with different molecular weights via electrified tungsten filament depolymerization: (1)

original PE; (2) condensed PE; (3) PE model compound (*n*-triacontane). (**E**) Comparison of the depolymerization performances, including C_2H_4 selectivity and C_2H_4 formation rate normalized by surface area, of conventional catalytic pyrolysis and this work.

Along with the gas products, condensed solid products were also observed (fig. S4). We characterized the collected solid product and compared it to the original PE structure. Elemental analysis (EA) showed that the condensed solid product and the original PE had almost identical carbon and hydrogen contents and even similar levels of slight impurity elements (oxygen, nitrogen, and sulfur) (fig. S5 and table S1). In the Raman spectra (Fig. 2B and table S2), the condensed solid product not only preserved the carbon-carbon bonding skeleton of PE, but also displayed full consistency with the original PE in the rocking, twisting, wagging, bending, and stretching of the CH_2 groups. Note that we characterized the PE and solid products at different locations, and the results all showed a high degree of consistency (figs. S6 and S7). The organic functional groups and the chemical state of the carbon elements were also identical to the original PE by Fourier transform infrared (FTIR) spectroscopy (fig. S8) and X-ray photoelectron spectroscopy (XPS) (fig. S9), confirming that the chemical structure of the solid product was the same as PE. This means that the product can be recycled and reused for the subsequent conversion (Fig. 2C), and the process would convert plastic fully to ethylene-rich gas products after multiple runs (fig. S10).

The mass fraction of carbon recovered in the gas form is less than 10% per reaction run (fig. S11), the rest being recovered PE. Despite that, the method offers an exceptional C_2H_4 formation rate. Operating in only 10 seconds, our method achieves a C_2H_4 monomer formation rate, normalized by the surface area of the filament, of 4×10^5 mmol m^{-2} h^{-1}, significantly higher than literature-reported rates (typically $<2 \times 10^3$ mmol m^{-2} h^{-1}). Furthermore, the monomer formation rate for this method was calculated based on a 10-second operation time, which means the reaction rate is likely to be underestimated, since the actual reaction time does not exceed 1 second.

The electrified tungsten filament method demonstrates strong versatility, achieving C_2H_4 monomer selectivities of approximately 47–51% for PE across various molecular weights (Fig. 2D), including original PE, condensed PE, and PE model compound. Unlike conventional thermal catalytic pyrolysis processes, which often suffer from the formation of liquid and solid byproducts like tar and coke, this method maintains high overall selectivity due to the absence of liquid and solid byproducts. Thus, the C_2H_4 monomer selectivity via this method has exceeded those of the optimized catalytic pyrolysis studies of PE reported in the literature (generally <20%) (Fig. 2E and table S3).

Transformation dynamics based on temperature and flow fields

To analyze the transformation dynamics of PE in the light bulb-like reactor, we employed computational fluid dynamics (CFD) simulations focusing on temperature and flow fields. These simulations reveal that, like a light bulb, the reactor remains predominantly at room temperature immediately after turning on, with only the tungsten filament reaching high temperatures (Fig. 3A). Under this operation condition, this reactor creates a sharp temperature gradient ($>10^6$ °C m^{-1}) within less than 1 mm of the filament in just 0.1 seconds (Fig. 3B). The depolymerization of PE to C_2H_4 at an elevated temperature of 1250 °C is thermodynamically favorable and has a considerable kinetic rate. Thus, PE not only melts and evaporates rapidly near the surface of the tungsten filament, but also instantly depolymerizes to C_2H_4 monomer when the reactor is activated. The

high-temperature zone favorable for PE depolymerization to C_2H_4 expands slightly during the 10-second operational period, while maintaining a favorable temperature gradient.

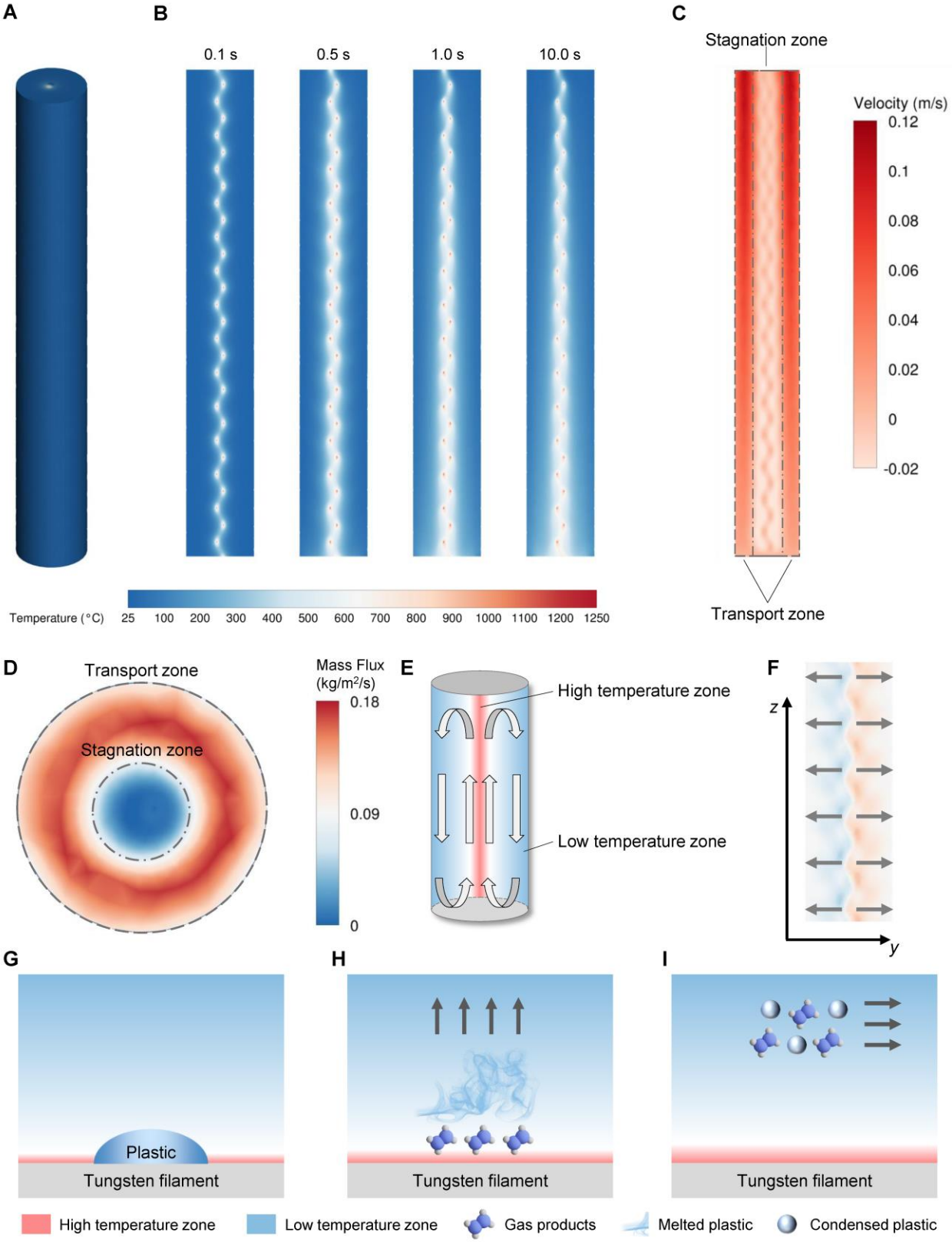

Fig. 3. Transformation dynamics of plastic depolymerization on electrified tungsten filament. (**A**) Three-dimensional transient temperature distribution inside the reactor at the operation time of 0.1 s. (**B**) Two-dimensional transient temperature distributions of the axial cross-section at different time scales. Both (A) and (B) are based on the temperature legend below. (**C**) Two-dimensional transient distribution of axial velocity in the axial cross-section at the operation time of 0.1 s. (**D**) Two-dimensional transient distribution of cumulative mass flux from inlet to outlet of the reactor at the operation time of 0.1 s. (**E**) Schematic of the fluid path in a typical Clusius-Dickel thermal diffusion column. The Clusius-Dickel thermal diffusion column can be regarded as the reactor in which both the inlet and outlet velocities are set to 0. (**F**) Two-dimensional transient distribution of the flow field in the y-direction at the operation time of 0.1 s. The light orange color represents the positive direction, and the light blue color represents the negative direction (see fig. S12 for the full-scale and detailed information). (**G** to **I**) Schematic diagrams of the control mechanism for converting plastic to gaseous products and partially retaining as condensed plastic. (**G**) Before reaction; (**H**) reaction and radial transport; (**I**) axial transport.

We further analyzed the axial velocity distribution inside the reactor to elucidate the impact of the flow field (Fig. 3C). Different velocity fields emerged across the radial direction. Notably, a stagnation zone formed around the central high-temperature region near the tungsten filament, characterized by near-zero velocities and even a tendency to form a reflux zone. This central stagnation caused increased axial velocities near the cooler walls, directing all mass transport through these lower-temperature areas. This phenomenon was also manifested in the mass flux (Fig. 3D), except for the decrease in velocity and mass transfer due to friction and fluid viscosity in a tiny region near the wall (<1 mm).

The reactor resembles a Clusius-Dickel thermal diffusion column (*32*, *33*), which will naturally bring about mass transport in the axial direction opposite to the direction of gravity (Fig. 3E). By balancing this movement with the carrier gas against the thermal diffusion, we maintained stagnation in the high-temperature center while inducing a strong outward radial velocity due to the temperature gradient (Fig. 3F and fig. S12). Initially, the tightly coated plastics on the tungsten filament respond instantly to the high temperatures: melting, evaporating, and partially depolymerizing (Fig. 3G and 3H). The fast removal of products from the reaction zone by the controlled flow field, and the rapid condensation of plastic vapors in the cold zone, ensure high selectivity and efficiency in the depolymerization process (Fig. 3I).

Chemical mechanism of polyethylene depolymerization

We used a model compound (*n*-triacontane) as the reactant to investigate the chemical depolymerization mechanism. For the depolymerization of PE, unzipping, i.e., successive chain-end β-scission, is more effective in generating C_2H_4 monomer than random β-scission and backbiting-induced mid-chain β-scission (*34*-*37*). If the mechanism mainly follows random β-scission, the C_2H_4 selectivity of PE pyrolysis will increase significantly as the molecular weight of the polymer decreases, but in fact the C_2H_4 selectivity produced by the model compound is not very different from that obtained by direct conversion of PE plastic (Fig. 2D). This phenomenon indicated that β-scission at the chain end is the primary mechanism for the formation of C_2H_4 monomer. By characterizing the condensed solid product of the reaction of *n*-triacontane by gas chromatography-mass spectrometry (GC-MS), we also did not find any obvious formation of intermediate length alkanes or olefins (e.g., *n*-pentadecane and *n*-pentadecene), which further

suggested that the mechanism of chain-end β-scission played a dominant role in this process (figs. S13 and S14).

The structures of PE before and after the reaction also provide clues for the reaction mechanism. While the solid-state ^{13}C nuclear magnetic resonance (NMR) results indicated that the original PE and the condensed PE maintained a highly unified structure (fig. S15A and fig. S16A), fine analysis by split-peak fitting revealed a reduced share of amorphous PE on the ^{13}C NMR spectra, suggesting that the amorphous PE decomposed first during the reaction (fig. S15B, fig. S16B, table S4 and table S5). On the ^{1}H NMR spectra, we captured a certain degree of increase in the percentage of -CH_3 end groups of the reacted PE, compared to the initial PE, which indicated that a slight breakage of the PE long chain still occurred in the solid phase (fig. S17, fig. S18, table S6, and table S7). We also compared the molecular weight distributions of the original PE and the condensed PE by high-temperature gel permeation chromatography (HT-GPC) and indeed found a slight decrease in the molecular weight of the latter (fig. S19 and table S8). This phenomenon further confirmed the possibility of the chain-end β-scission mechanism, consistent with previously reported results (*34*, *38*, *39*). In the chain-end β-scission process, C_2H_4 is the dominant reaction product, while in the subsequent process, some of the C_2H_4 that did not have time to be transported by the flow field in time to the low-temperature region gave rise to secondary transformations, then contributing to other hydrocarbons in the gaseous product (fig. S20).

Application potential and scalability

Our method has potential for continuous plastic depolymerization. For example, Fig. 4A illustrates a proposed Ferris wheel-like continuous plant concept. The unit consists of three parts, i.e., a plastic melting system, a tungsten rotary coating system, and a reaction system. In this continuous reaction unit, PE plastics of any shape are melted without mechanical pre-processing (e.g., shredding). Through the rotation of a Ferris wheel-like rotary coating system, tungsten filament is submerged into molten plastic for coating. When the tungsten filament, already coated with plastic, reaches the right side of the rotary coating system, it is delivered into the reaction system for depolymerization reaction, and sent back for the next round of coating after the reaction.

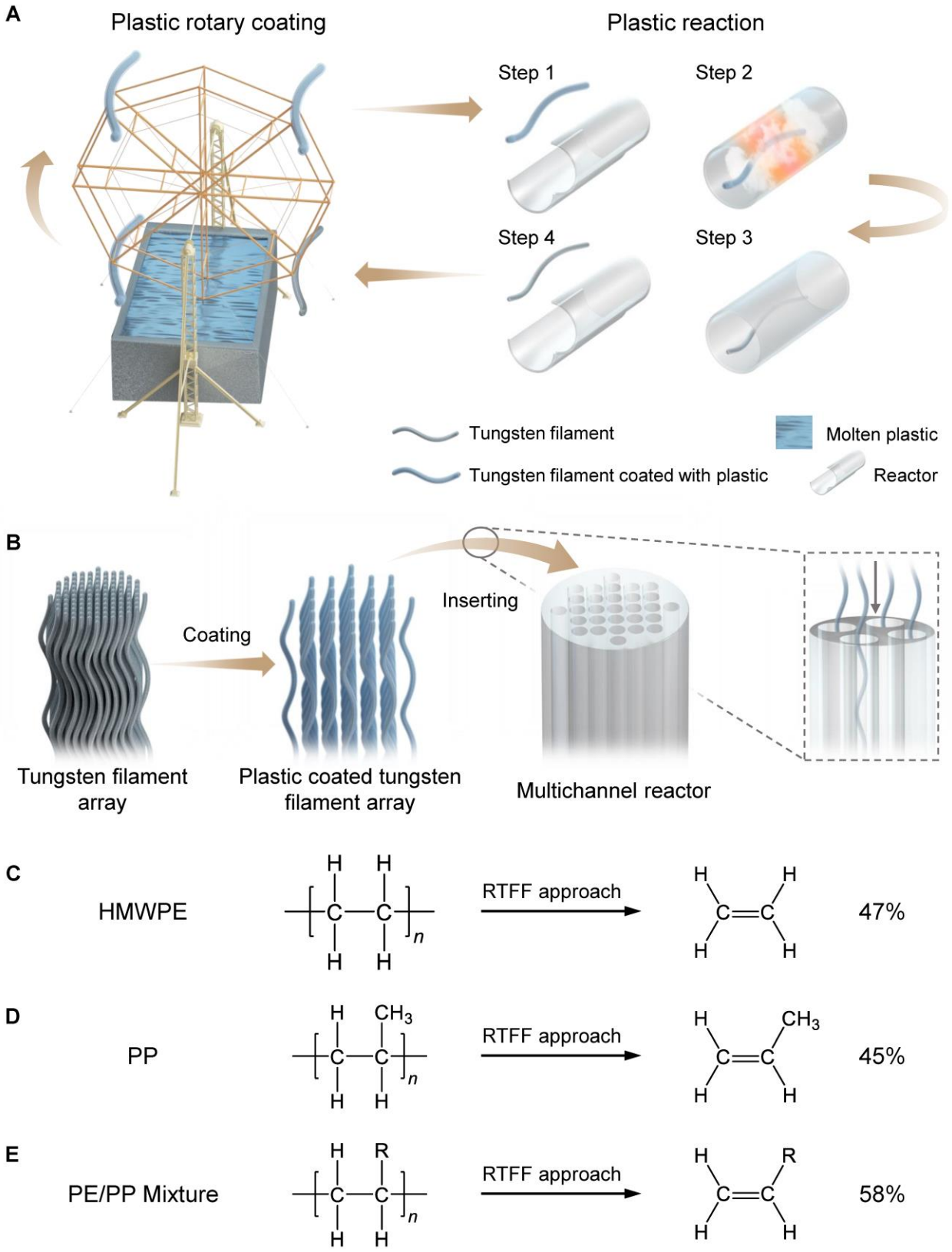

Fig. 4. Application potential of the electrified tungsten filament approach. (**A**) Schematic of a proposed Ferris wheel-like continuous plant concept based on the electrified tungsten filament approach for plastic depolymerization. This continuous plant concept allows for the continuous

depolymerization of plastic by means of multiple tungsten filaments rotating successively between the plastic melting pool and the reaction system. (**B**) Potentially larger scale industrial application of the electrified tungsten filament method by incorporating current industrial process that involves metal processing, enameled wire processing, and mechanical processing. (**C**) Depolymerization reaction of high-molecular-weight PE (HMWPE) converted to C_2H_4 monomer by electrified tungsten filament approach with a selectivity of 47%. (**D**) Depolymerization reaction of PP converted to C_3H_6 monomer by electrified tungsten filament approach with a selectivity of 45%. (**E**) Depolymerization reaction of PE/PP mixture converted to C_2H_4 and C_3H_6 monomers by electrified tungsten filament approach with a combined selectivity of 58%. The group R represents H and CH_3.

To investigate the feasibility of this continuous system concept, we performed relevant validations at the laboratory scale. By using commercially available industrial-grade tungsten filaments for cyclic experiments of the depolymerization reaction, we found that the tungsten filaments presented a stable weight (fig. S21) and maintained consistent selectivity performance (47–50%) (fig. S22) after several experiments. The results of scanning electron microscopy (SEM) energy dispersive X-ray spectroscopy (SEM-EDS) at different scales illustrated that the microscopic morphology and elemental distribution of the tungsten filaments did not show significant changes during the reaction process (figs. S23 to S31), and the slight changes in the surface were attributed to the recrystallization of tungsten at elevated temperatures (*40*, *41*). Moreover, we observed from the XPS results that the tungsten oxide on the surface of the tungsten filament was slightly reduced to metallic tungsten (fig. S32 and table S9), which was attributed to trace amounts of hydrogen produced during the plastic depolymerization reaction (e.g., C_2H_4 dehydrogenation) (*42*). In practice, the trace reduction reaction can be counteracted with trace amounts of oxygen during the reaction to bring about oxidation and increase oxygen tolerance. Additionally, we investigated whether prolonged melting would have an effect on the structure of PE. The results of HT-GPC showed that melting for up to 100 h under an atmosphere of air only slightly reduced the molecular weight of PE (fig. S33 and table S8), which further proves the feasibility of the above concept of continuous operation.

The process is scalable by incorporating existing industrial equipment. For example, tungsten filament array can be produced in large quantities to achieve high-volume plastic coating (Fig. 4B). In the subsequent process, plastic-coated tungsten filament array can be installed in a multichannel reactor for simultaneous conversion in large batches and recycled. The method has also shown versatility in depolymerizing various polyolefins, achieving monomer selectivities of 47% for high-molecular-weight PE (HMWPE) and 45% for PP, and a combined selectivity of 58% for a PE and PP mixture, with proportions of 33% ethylene and 25% propylene (Figs. 4C to 4E).

Numerical simulations confirm that the temperature and flow fields generated by the electrified tungsten filament method are effective across a broad temperature range from 500 to 3000 °C, suggesting potential applicability to diverse reaction systems and research fields (figs. S38 to S41). The method's adaptability extends to other metals like molybdenum and nickel, although optimizations are to be achieved in future studies (fig. S42).

Discussion

In summary, we develop an electrified tungsten filament method for depolymerizing polyolefin plastics into olefin monomers. We achieve an ethylene monomer selectivity of 48% in the depolymerization of polyethylene, improving more than twice relative to the conventional

catalytic pyrolysis. Polyethylene and polypropylene of different molecular weights and their mixtures can be depolymerized by this process. Polyolefin plastics are melted, evaporated and depolymerized within 1 s of the tungsten filament being activated. The ultra-fast heat transfer characteristics and multi-temperature-zone environment control and prevent undesirable side reaction. The introduced flowing inert gas creates a characteristic flow field opposite to the temperature, which in turn enables the transfer and control of the plastic between different temperature zones. This technology shows potential for global plastic waste management. Its advantages include high monomer selectivity, high reaction rate, potential for scaling up, and versatility in terms of applicable polyolefins and conditions. Recovered olefin monomers are useful feedstock for plastic repolymerization or downstream chemical industries, offering new opportunities to mitigate the carbon footprint of the current petroleum-based chemical industry.

Methods

Depolymerization of polyethylene

Polyethylene was depolymerized by means of a tungsten filament loaded inside the reactor. In a typical experiment, polyethylene powder was first placed in a beaker, which was heated until the polyethylene powder in the beaker melted to a molten state (i.e., a clear, transparent liquid). A commercially available piece of industrial-grade tungsten filament with a diameter of 0.1 mm was taken and the tungsten filament was bent into a helical shape to prepare for the subsequent flow field. The tungsten filament was weighed before use. The cooled tungsten filament was then quickly submerged in liquid polyethylene in the molten state and quickly taken out for cooling to achieve the coating of the polyethylene on the surface of the tungsten filament. The total weight of the coated tungsten wire and the polyethylene plastic was measured, and the amount of polyethylene plastic coated was determined by comparing the weight of the coated tungsten filament with that of the uncoated tungsten filament. The ends of the tungsten filament coated with polyethylene were then secured to the OT-type open-end copper fittings. The copper fittings at each end were bolted to the copper wire connectors in the flange seals on each side. Here the outer end of the copper wire was directly connected to a small direct current (DC) power supply for subsequent lighting of the tungsten filament. The entire plastic-coated tungsten filament was placed in the center of a quartz tube, and the tungsten filament was secured and adjusted on both sides by means of copper wires. The quartz tube was sealed to the flange seals by four fluorinated rubber O-rings. On the other side of the inlet flange seal a tee line was connected, one of which was used for the connection of the copper wires and the other for feeding the carrier gas into the reactor. The flange seal at the outlet was similar, and the tee line was used for the transmission of the circuit and the outflow and collection of the gas.

After installing the reaction apparatus, the reactor inlet was first closed, and a vacuum pump was connected to the outlet. The vacuum pump was turned on to remove air from inside the reactor and the vacuum inside the reactor was balanced with argon gas from upstream and repeated five times. Afterward, the reactor was steadily fed with an argon carrier gas for one hour to ensure the removal of impurity gases, such as oxygen, from the reaction chamber. Next, a gas sample bag was attached to the back end of the reactor and the small DC power supply was turned on to illuminate the tungsten filament. The temperature of the tungsten filament was calculated from the difference in resistance at room temperature and during operation and the corresponding resistance temperature coefficient (*43*, *44*). The resistance at room temperature was directly calculated from the length, diameter, and resistivity and verified with a multimeter. The resistance during operation

was calculated from voltage and current. After 10 seconds, the tungsten filament was turned off and the upstream argon gas was continuously purged to ensure efficient collection of the gaseous products generated by the reaction. Since gas production during the reaction is a transient and variable process, all gas products were averaged over time and space by means of a gas sample bag to evaluate and compare the gas products produced by each reaction. A thin layer of aluminum foil was placed against the inner wall of the quartz tube to collect the condensed polyethylene solids after the reaction.

Characterization techniques

Elemental analysis (ThermoFisher Scientific FlashSmart CHNS Elemental Analyser) was used to analyze the elemental composition of polyethylene and its solid products. To determine the molecular structures of the samples, Raman spectra (Renishaw inVia Qontor confocal Raman microscope) outfitted with a Renishaw Centrus 4AUL40 detector was used. The FTIR spectroscopy were collected on an Agilent Cary 660 spectrometer to analyze the organic functional groups in the polyethylene and its solid products. In order to investigate the surface chemical states of the polymers and tungsten filaments, XPS analysis was conducted using a Kratos AXIS ULTRADLD instrument manufactured by Shimadzu, Japan. ^{1}H magic-angle spinning (MAS) solid-state NMR spectroscopy and ^{13}C cross-polarization (CP)/MAS/total suppression of sidebands (TOSS) solid-state NMR spectroscopy measurements were conducted on a Bruker Avance NEO 500MHz NMR spectrometer. HT-GPC (Agilent PL-GPC 220) experiments were performed to obtain the molecular weight distributions of the polymers. To determine the composition of the gas products, GC-FID (Agilent 8890) with a GS-Alumina KCl porous layer open tubular (PLOT) column was used. GC-MS (Agilent 7890A and 5975C system) with a DB-5 standard polysiloxane column was utilized to detect the specific chemical composition of the organic solutions of the model components. SEM (JSM-7610F Plus, JEOL, Japan) and EDS (X-Max^{N}, Oxford Instruments) were conducted to observe the microscopic morphology and elemental distribution of the tungsten filaments.

More detailed experimental methods are described in the Supplementary Methods.

References and Notes

1. R. Geyer, J. R. Jambeck, K. L. Law, Production, use, and fate of all plastics ever made. *Sci. Adv.* **3**, e1700782 (2017).
2. A. Ahrens *et al.*, Catalytic disconnection of C–O bonds in epoxy resins and composites. *Nature* **617**, 730-737 (2023).
3. R. W. Clarke *et al.*, Dynamic crosslinking compatibilizes immiscible mixed plastics. *Nature* **616**, 731-739 (2023).
4. J. R. Jambeck *et al.*, Plastic waste inputs from land into the ocean. *Science* **347**, 768-771 (2015).
5. R. C. Thompson *et al.*, Lost at sea: Where is all the plastic? *Science* **304**, 838-838 (2004).
6. B. Carney Almroth *et al.*, Understanding and addressing the planetary crisis of chemicals and plastics. *One Earth* **5**, 1070-1074 (2022).
7. M. A. Browne *et al.*, Accumulation of microplastic on shorelines woldwide: Sources and sinks. *Environ. Sci. Technol.* **45**, 9175-9179 (2011).
8. J. Kim, J. Jang, T. Hilberath, F. Hollmann, C. B. Park, Photoelectrocatalytic biosynthesis fuelled by microplastics. *Nat. Synth.* **1**, 776-786 (2022).

9. K. P. Sullivan *et al.*, Mixed plastics waste valorization through tandem chemical oxidation and biological funneling. *Science* **378**, 207-211 (2022).
10. F. Zhang *et al.*, Polyethylene upcycling to long-chain alkylaromatics by tandem hydrogenolysis/aromatization. *Science* **370**, 437-441 (2020).
11. M. Liu, X. Wu, P. J. Dyson, Tandem catalysis enables chlorine-containing waste as chlorination reagents. *Nat. Chem.* **16**, 700-708 (2024).
12. J. M. Garcia, M. L. Robertson, The future of plastics recycling. *Science* **358**, 870-872 (2017).
13. Z. O. G. Schyns, M. P. Shaver, Mechanical Recycling of Packaging Plastics: A Review. *Macromol. Rapid Commun.* **42**, 2000415 (2021).
14. S. Kakadellis, G. Rosetto, Achieving a circular bioeconomy for plastics. *Science* **373**, 49-50 (2021).
15. K. M. Van Geem, Plastic waste recycling is gaining momentum. *Science* **381**, 607-608 (2023).
16. C. Jehanno *et al.*, Critical advances and future opportunities in upcycling commodity polymers. *Nature* **603**, 803-814 (2022).
17. L. D. Ellis *et al.*, Chemical and biological catalysis for plastics recycling and upcycling. *Nat. Catal.* **4**, 539-556 (2021).
18. H. Li *et al.*, Hydroformylation of pyrolysis oils to aldehydes and alcohols from polyolefin waste. *Science* **381**, 660-666 (2023).
19. H. Lu *et al.*, Machine learning-aided engineering of hydrolases for PET depolymerization. *Nature* **604**, 662-667 (2022).
20. V. Tournier *et al.*, An engineered PET depolymerase to break down and recycle plastic bottles. *Nature* **580**, 216-219 (2020).
21. C. C. Chen *et al.*, General features to enhance enzymatic activity of poly(ethylene terephthalate) hydrolysis. *Nat. Catal.* **4**, 425-430 (2021).
22. S. Zhang *et al.*, Depolymerization of polyesters by a binuclear catalyst for plastic recycling. *Nat. Sustain.* **6**, 965-973 (2023).
23. R. J. Conk *et al.*, Catalytic deconstruction of waste polyethylene with ethylene to form propylene. *Science* **377**, 1561-1566 (2022).
24. W. Zhang *et al.*, Low-temperature upcycling of polyolefins into liquid alkanes via tandem cracking-alkylation. *Science* **379**, 807-811 (2023).
25. K. Lee, Y. Jing, Y. Wang, N. Yan, A unified view on catalytic conversion of biomass and waste plastics. *Nat. Rev. Chem.* **6**, 635-652 (2022).
26. L. H. Kugelmass, C. Tagnon, E. E. Stache, Photothermal Mediated Chemical Recycling to Monomers via Carbon Quantum Dots. *J. Am. Chem. Soc.* **145**, 16090-16097 (2023).
27. W.-T. Lee *et al.*, Mechanistic classification and benchmarking of polyolefin depolymerization over silica-alumina-based catalysts. *Nat. Commun.* **13**, 4850 (2022).
28. K. Zheng *et al.*, Progress and perspective for conversion of plastic wastes into valuable chemicals. *Chem. Soc. Rev.* **52**, 8-29 (2023).
29. M. Häußler, M. Eck, D. Rothauer, S. Mecking, Closed-loop recycling of polyethylene-like materials. *Nature* **590**, 423-427 (2021).
30. G. W. Coates, Y. D. Y. L. Getzler, Chemical recycling to monomer for an ideal, circular polymer economy. *Nature Reviews Materials* **5**, 501-516 (2020).
31. Q. Dong *et al.*, Depolymerization of plastics by means of electrified spatiotemporal heating. *Nature* **616**, 488-494 (2023).
32. G. Müller, G. Vasaru, The Clusius-Dickel Thermal Diffusion Column – 50 Years after its

Invention. *Isotopenpraxis* **24**, 455-464 (1988).
33. I. Budin, R. J. Bruckner, J. W. Szostak, Formation of Protocell-like Vesicles in a Thermal Diffusion Column. *J. Am. Chem. Soc.* **131**, 9628-9629 (2009).
34. N. A. Sezgi, W. S. Cha, J. M. Smith, B. J. McCoy, Polyethylene Pyrolysis: Theory and Experiments for Molecular-Weight-Distribution Kinetics. *Ind. Eng. Chem. Res.* **37**, 2582-2591 (1998).
35. X. Liu *et al.*, Study of high density polyethylene (HDPE) pyrolysis with reactive molecular dynamics. *Polym. Degrad. Stab.* **104**, 62-70 (2014).
36. W. C. McCaffrey, D. G. Cooper, M. R. Kamal, Tertiary recycling of polyethylene: mechanism of liquid production from polyethylene by thermolysis/reactive distillation. *Polym. Degrad. Stab.* **62**, 513-521 (1998).
37. Z. Xu *et al.*, Chemical upcycling of polyethylene, polypropylene, and mixtures to high-value surfactants. *Science* **381**, 666-671 (2023).
38. D. Zhao, X. Wang, J. B. Miller, G. W. Huber, The Chemistry and Kinetics of Polyethylene Pyrolysis: A Process to Produce Fuels and Chemicals. *ChemSusChem* **13**, 1764-1774 (2020).
39. Y. Kodera, B. J. McCoy, Distribution Kinetics of Polymer Thermogravimetric Analysis: A Model for Chain-End and Random Scission. *Energy Fuels* **16**, 119-126 (2002).
40. A. Šestan, P. Jenuš, S. N. Krmpotič, J. Zavašnik, M. Čeh, The role of tungsten phases formation during tungsten metal powder consolidation by FAST: Implications for high-temperature applications. *Mater. Charact.* **138**, 308-314 (2018).
41. H. Yu, S. Das, J. Liu, J. Hess, F. Hofmann, Surface terraces in pure tungsten formed by high temperature oxidation. *Scripta Mater.* **173**, 110-114 (2019).
42. T. Kuroki, T. Sawaguchi, S. Niikuni, T. Ikemura, Mechanism for long-chain branching in the thermal degradation of linear high-density polyethylene. *Macromolecules* **15**, 1460-1464 (1982).
43. P. D. Desai, T. K. Chu, H. M. James, C. Y. Ho, Electrical Resistivity of Selected Elements. *J. Phys. Chem. Ref. Data* **13**, 1069-1096 (1984).
44. W. E. Forsythe, E. M. Watson, Resistance and Radiation of Tungsten as a Function of Temperature. *J. Opt. Soc. Am.* **24**, 114-118 (1934).

Acknowledgments: The authors acknowledge the support from the National University of Singapore Department of Chemical and Biomolecular Engineering and Centre for Hydrogen Innovations. This work was supported by the NRF Investigatorship (NRF-NRFI07–2021–0006).

Author contributions: N.Y. conceived and supervised the project. S.Y., S.W., and H.L. built the reaction system. S.Y. carried out the experiments, conducted the characterization, and analyzed the data. S.Y. carried out the numerical simulation. S.Y. and H.L. made the video. S.Y. and N.Y. wrote the paper.

Competing interests: N.Y. and S.Y. are inventors on patent application pertaining to this work.

Data and materials availability: All data are available in the main text or the supplementary materials.